RSC Advances

ROYAL SOCIETY OF CHEMISTRY

www.rsc.org/advances

Journal Name

ARTICLE

A new strategy of spray pyrolysis to prepare porous carbon nanosheet with enhanced ionic sorption capacity

Received 00th January 20xx,
Accepted 00th January 20xx

DOI: 10.1039/x0xx00000x

www.rsc.org/

Pung Ho Kim and Kyeong Youl Jung*

Abstract In this work, a simple and efficient spray pyrolysis process was developed in order to easily control the microstructure of carbon particles prepared from sucrose as a carbon source. The key idea of this work is to modify the sucrose-based aqueous spray solution with organic additives, polyethylene glycol (PEG) and carbohydrazide, as a structure-controlling agent. It was found that the use of both PEG and carbohydrazide as the organic additive makes it possible to produce carbon nanosheets similar with multi-layer graphene oxides. In addition, the organic additives were helpful for increasing the specific surface area of carbon powders. Carbon nanosheets had improved ion-sorption capacitance compared with porous carbon spheres with the filled morphology or the hollow structure due to the increase of ion-accessible surface area. From the electrochemical characterization, the carbon nanosheets with the structure like a graphene oxide, which could be successfully synthesized by the suggested new strategy, were revealed to be most profitable to the electrode materials with high ion-sorption capacitance.

1. Introduction

Porous carbon materials (PCMs) have gained a great attention due to their excellent properties in various research fields, such as energy storage,[1-4] pollutant separation,[5-8] and catalysis.[9-11] In particular, PCMs have been used as the major electrode materials in energy-related technologies including Li-ion battery,[12-14] supercapacitor[15-18] and capacitive deionization.[19-22] The main key issues in the synthesis of porous carbons are to control the pore size/distribution, the particle size and the surface area/properties. The required properties of PCMs are different with application areas. In general, carbons need to have high surface area and good conductivity. Commercially available activated carbons have been used as electrode materials because they have high surface area, excellent chemical stability, and good conductivity. Activated carbons, however, have mostly micropores which are not good for ion diffusion and adsorption. To achieve high performance, the large amount of ions should enable to be adsorbed on or rapidly inserted into the electrode materials. That is, it is necessary for carbons to have an adequate pore size and structure in order to give good ion accessibility as well as excellent ion transport.

Mesoporous carbons have good pore structure for ion diffusion/adsorption, but they show relatively low electric conductivity. To overcome this drawback, high conductive carbons including carbon nanotube (CNT) and graphene are frequently mixed with mesoporous carbons as a composite electrode. Also, mesoporous carbon-coated graphene or graphitic nanosheets have gain attention as attractive electrode materials possessing excellent transport properties as well as high capacitance.[23-25] Thus, a lot of efforts have been made to develop new synthetic methods which make it possible to design the porous carbons to have the proper properties met with this requisition. Representative methods used to prepare porous carbons are chemical/physical activation,[26-28] sol-gel,[29] template-based carbonization,[30-34] and chemical vapor decomposition.[35-37] In terms of achieving fast ion diffusion or adsorption, mesoporous carbon (MC) is considered as a potential candidate for electrode materials. To synthesize structurally ordered-mesoporous carbons, sacrificial rigid templates including silica, zeolite and metal-organic framework (MOF) have been used. However, the inorganic templates are expensive and require corrosive chemicals to remove them, which act a bottle neck for industrial scale-up and commercialization. Recently, the ultrasonic spray pyrolysis has attracted great attention as a promising process to synthesize various carbon-based porous materials due to the advantages of its simplicity, continuous production, and one-pot process.[38-47] A typical spray pyrolysis process produces particles via a droplet-to-particle conversion mechanism. The process has the advantage of controlling the composition of multi-component materials, easily and precisely. Thus, the spray pyrolysis has been extensively utilized to design a variety of functional materials including phosphors,[48-50] porous oxides,[51-53] and organic-inorganic composites.[54-56]

When porous carbon materials are prepared by the spray pyrolysis, the particle size, morphology and porosity are controllable by the characteristics of carbon precursor, the properties of precursor solution, and the operation conditions (e.g. reactor temperature and gas flow rate). The carbon precursors frequently used are sucrose, block copolymer and phenolic resin.

[a] Department of Chemical Engineering, Kongju National University, 1223-4 Cheonan-Daero, Seobuk-gu, Cheonan, Chungnam, 331-717, Republic of Korea

† Footnotes relating to the title and/or authors should appear here.
Electronic Supplementary Information (ESI) available: [details of any supplementary information available should be included here]. See DOI: 10.1039/x0xx00000x

*Corresponding author (Kyoeng Youl Jung)
E-mail: kyjung@kongju.ac.kr
Tel: +82-41-521-9365
Fax: +82-41-554-2640

Porous carbon particles prepared by spray pyrolysis have generally spherical morphologies, but the pore structures are varied by the type of precursors. For example, when sucrose is used as the carbon source, the resulting carbons have different pore structures depending on the type of catalyst (sodium carbonate or bicarbonate) and its concentration.[40] Recently, the hierarchical porous carbon structure in which inside meso- or macropores are surrounded by outer micropores was synthesized by the spray pyrolysis and applied to the electrode materials of lithium-sulfur battery.[57] The unique hierarchical pore structure of carbon spheres prepared by the spray pyrolysis was proved to have excellent electrochemical performance. Occasionally, the spray pyrolysis produces non-spherical and unusual nanostructured carbon particles. For example, the carbon particles prepared by using alkali propiolates ($HC{\equiv}CCO_2M$, M = Li, Na, and K) as the carbon source was reported to have Janus, jellyfish, and bowl-like microstructures.[58] On the base of the previous literatures, the spray pyrolysis is a powerful tool for the preparation of carbon-based functional materials.

In this work, we report a new strategy able to easily control the nanostructure of carbon particles prepared by the spray pyrolysis. Inexpensive sucrose was used as a carbon source and organic additives was used as a structure-controlling agent. The proposed method is able to make hollow-structured carbon particles without the use of templates by simply adding organic additives to the sucrose-based precursor solution. Until now, to our best knowledge, there is no report of the direct synthesis of carbon nanosheets like multi-layered graphene oxides via the spray pyrolysis process. Herein, we explored a facile synthetic technique to obtain carbon nanosheet through the spray pyrolysis. The key idea is to use two different organic additives, polyethylene glycol (PEG) and carbohydrazide. Based on the general mechanism of particle formation in spray pyrolysis, the hollow carbon particles with a very thin layer were prepared and easily fractured into carbon nanosheet via a ultrasonic post-washing process. Furthermore, the developed method is simple and effective for increasing the specific surface area of porous carbon particles. For the prepared porous carbon particles with different morphologies, the ionic sorption capacitance was investigated in order to give information on the morphology importance of porous carbon materials when they are used as electrode materials for ionic sorption separation or energy-storage devices.

2. Experimental

2.1 Preparation of carbon via spray pyrolysis

Sucrose and sodium carbonate were used as the precursors of carbon and catalyst, respectively. Polyethylene glycol (PEG 200) and carbohydrazide were used as an organic additive. All chemicals were purchased from Aldrich and used directly without any further purification. Porous carbon powders were synthesized using a conventional spray pyrolysis consisting of an ultrasonic aerosol generator with 6 vibrators of 1.7 MHz, a quartz tube of 55 mm (diameter) × 1200 mm (length), and a Teflon bag filter. The schematic diagram of the spray-pyrolysis process was shown in Fig. S1.

Three different spray solutions were prepared by dissolving sucrose, sodium carbonate and PEG in purified water. The first solution was prepared by dissolving 85.5 g of sucrose and 47.7 g of sodium carbonate in 500 mL of purified water. To prepare the second solution, PEG was added to aqueous solution containing both sucrose (85.5 g) and sodium carbonate (47.7 g). In the second solution, the PEG weight was varied from 10 g (0.1M) to 70 g (0.7 M). The third solution was prepared by adding 22.5 g of carbohydrazide to the second solution containing 30 g of PEG. Thereafter, the spray solution was atomized by the ultrasonic aerosol generator, and the produced droplets were carried into the quartz reactor maintained at 800 °C by a nitrogen-gas flow of 10 L/min. To remove alkali salts, the as-prepared carbon powders were washed several times by using purified water. The carbon powder prepared without any additives (PEG or carbohydrazide) was denoted as SP1. The samples prepared from the spray solution containing PEG and PEG/carbohydrazide mixture were denoted as SP2 and SP3, respectively.

2.2 Characterization

The crystal structures of the carbon samples before and after the washing for the SP1 sample were identified using X-ray diffraction (XRD, Rigaku, MiniFlex600). The morphology and microstructure were investigated using field-emission scanning electron microscopy (FE-SEM, MIRA LMH, TESCAN) and transmission electron microscopy (TEM, Philips Tecnai F20). The structural information of the prepared carbon powders were investigated by measuring Raman spectra (ARAMIS, Horiba Jobin Yvon). The specific surface area was calculated using a Brunauer-Emmett-Teller (BET) method from nitrogen adsorption isotherm data.

To investigate the ionic-sorption capacitance and electrochemical properties, the cyclic voltammetry (CV) and electrical impedance spectroscopy (EIS) measurements were carried out in 0.5 M KCl solution using a three-electrode system, including the working electrode fabricated with the prepared carbon powder. A carbon-coated platinum rode and an Ag/AgCl electrode were used as a counter and a reference electrode, respectively. To prepare electrodes using the prepared carbon or commercially available activated carbon (ACP, CPE-21K, PCT Co., Korea), 1 g of polyvinylidene fluoride (PVdF, Mw = 530,000) and 20 g of di-methylacetamide (DMAc) were mixed with carbon powder (9 g) using a planetary centrifugal mixer (Thinky mixer, ARE-310) to make paste. Thereafter, the paste was casted as a film via a doctor-blade method on a graphite sheet (Dong-bang Carbon Co., Korea). Cyclic voltammetry was performed in the potential range from -0.5 V to 0.5 V (vs. Ag/AgCl) at a scan rate of 5 mV/s. The EIS analysis was carried out at frequencies ranging from 100 Hz to 20 mHz.

3. Results and discussion

3.1 Morphology and microstructure analysis

Fig. 1 shows XRD patterns of the as-prepared carbon powders (SP1) before the washing and the extract withdrawn from the solution obtained by the washing. The XRD peaks for the as-prepared carbon powders are corresponding to the crystalline of $Na_2CO_3{\cdot}H_2O$ and $Na_3H(CO_3)_2{\cdot}2HO$. The extract shows the peaks of monoclinic Na_2CO_3 phase. The XRD pattern of carbon spheres obtained after the washing was consistent with those of amorphous materials (Fig. S2). Therefore, the as-prepared powders are composites consisting of amorphous carbon and sodium carbonates (hydrate forms).

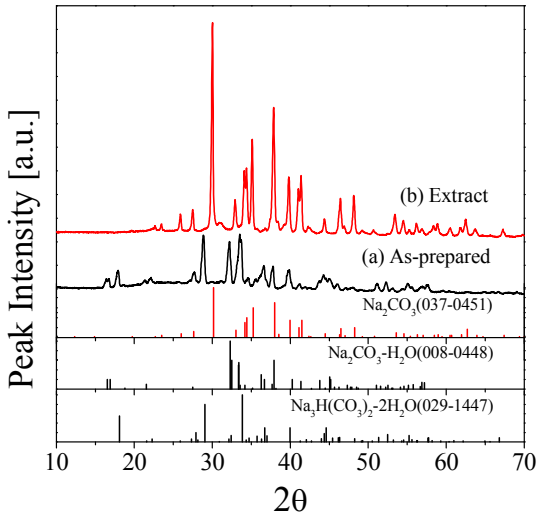

Fig. 1 XRD patterns for (a) as-prepared carbon particles (SP1) and (b) the extract obtained after the washing process.

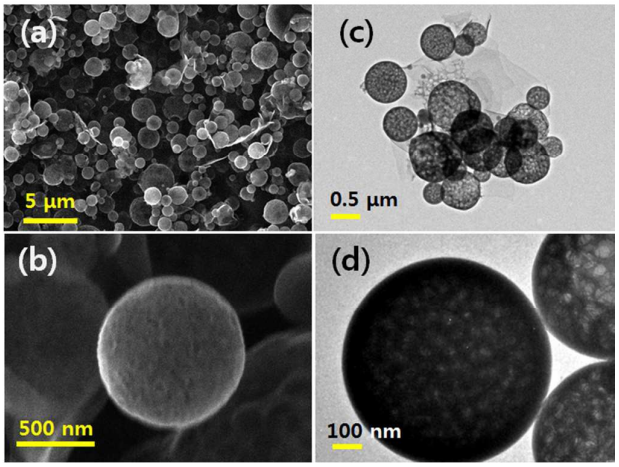

Fig. 2 SEM (a and b) and TEM (c and d) images of the carbon SP1

Fig. 2 shows the morphology and microstructure of the carbon powder (SP1) prepared by spray pyrolysis from the spray solution containing no organic additives (PEG or carbonhydrazide). The SEM images (Fig. 2a and b) indicate that the carbon powders were spherical and porous. The TEM images (Fig. 2c and d) clearly reveal the porous structure of spherical carbon spheres. In special, large pores were observed at the inside region of carbon spheres. The size of sodium carbonates plays a key role on generating the macro pores of carbon spheres (SP1). From the SEM images of carbon powders before the washing, which were shown in Fig. S3a, one can see nano-sized precipitates dispersed on the surface of carbon spheres. These nanoparticles are not observed after the washing (Fig. S3b). The effective removal of sodium carbonate could be identified by the EDX analysis (Fig. S4). Accordingly, the precipitated sodium carbonate is revealed to exist as nanoparticles which are removed by the washing step, generating the macropores observed in Fig. 2d. On the base of this observation through the SEM and TEM analysis, the mechanism for the generation of porous carbon spheres (SP1) in spray pyrolysis was shown in Scheme 1. As droplets are passing through the quartz reactor, the salt concentration increases due to the water evaporation. As a result, the sucrose and carbonates are precipitated as the composite powders (intermediate product). In this step, nano-sized sodium carbonate particles are formed within the whole particles. After that, sucrose is carbonized to form porous carbon spheres containing the nanoparticles of sodium-carbonate derivatives. The washing of as-prepared powder generates macro-sized inner pores by removing the sodium-carbonate derivatives.

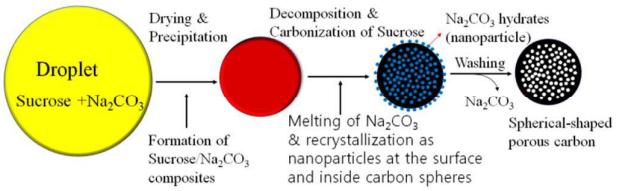

Scheme 1. Schematic diagram for the formation mechanism of porous carbon spheres with a filled morphology.

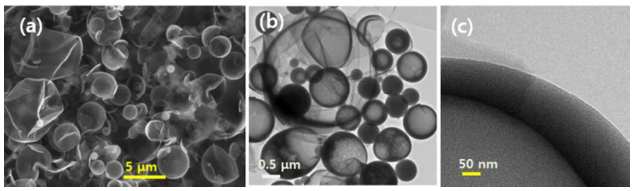

Fig. 3 SEM (a) and TEM (b and c) images of the carbon powder (SP2) prepared from the precursor solution containing PEG as an organic additive.

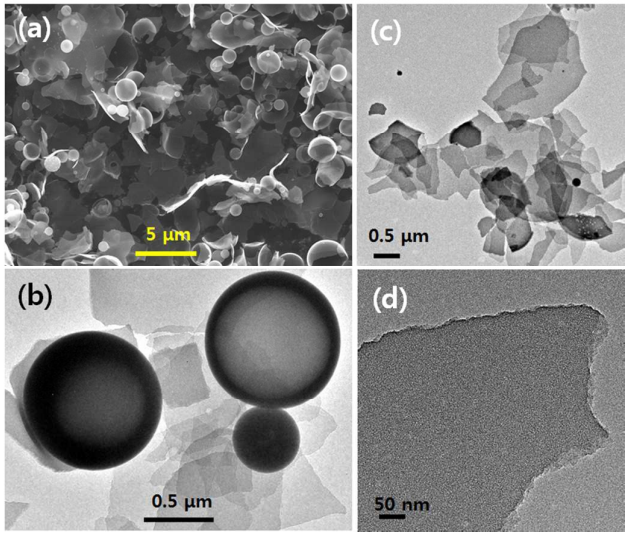

Fig. 4 SEM (a) and TEM (b – d) images for the carbon particles (SP3) prepared from the spray solution containing PEG and carbohydrazide as an organic additive.

Carbon particles were prepared by changing the concentration of PEG added to the spray solution. The PEG addition to the spray solution totally changes the microstructure of carbon spheres. Fig. 3 shows SEM and TEM images for the carbon powder (SP2) prepared

from the precursor solution containing PEG (0.3 M). The particle size is greater than that of the carbon (SP1) sample prepared without the PEG additive. When the PEG concentration was 0.3 M and larger, no big change in the particle size was observed (Fig. S5). As shown in the TEM images, the prepared carbon particles have hollow morphology. The shell layer is very porous and has the thickness of about 150 nm. From this result, PEG added to the spray solution plays a role of inflating the carbon particles. Fig. 4 shows SEM and TEM images of the carbon particles (SP3) prepared from the precursor solution containing both carbohydrazide and PEG. Most of carbon spheres are fractured as a nanosheet shape although some small particles still have hollow-structured morphology. The high-resolution TEM image for the fragmented carbon (Fig. 4d) indicates that the thickness is very thin and it seems like multi-layered graphene oxides. The hollow-structured small particles can be easily fragmented by increasing the ultrasonic washing time as shown in Fig. S6. From the results shown Fig. 3 and 4, it is clear that the morphology is easily controlled by only changing the types of organic additives added to the precursor solution when the carbon particles are prepared by spray pyrolysis.

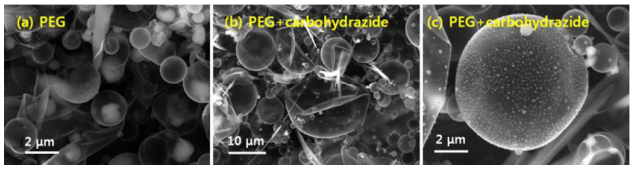

Fig. 5 SEM images of as-prepared carbon particles from the spray solution containing PEG (a) and PEG/carbohydrazide (b and c).

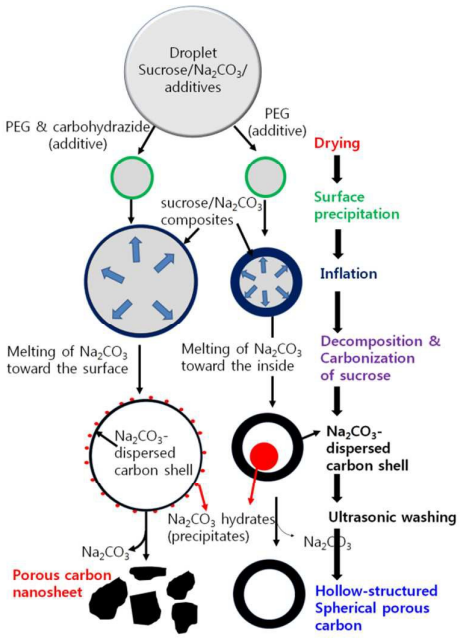

Scheme 2. Schematic diagram for the evolution of hollow morphology and carbon nanosheet.

The SEM analysis of the as-prepared carbon particles before the washing was carried out to investigate why the morphological difference is observed, and the results are shown in Fig. 5. For the case that only PEG is used, the as-prepared carbon spheres are hollow and the sodium carbonate is precipitated mostly at the inside of the spheres. For the case that both PEG and carbohydrazide are added to the spray solution, the as-prepared carbon particles have much larger size than that of the PEG-added carbon. Also, the precipitated sodium carbonates are dispersed at the thin shell layer of hollow carbon spheres. Scheme 2 is the schematic diagram for the evolution of hollow particles or carbon nanosheets. As water is evaporated, the concentration of both salts and organic additives first reaches the supersaturation points at the surface of droplet. As a result, the surface precipitation begins with forming a composite layer (sucrose/Na_2CO_3/organic additives) with the precursor solution at the inside of droplets. As the additional evaporation of inside water or the decomposition of organic elements proceeds, the inner pressure of droplets is elevated. As a result, the composite layer is inflated so that hollow composite particles are formed. In this step, the use of carbohydrazide with PEG more largely inflates the particles. Thereafter, the carbonization takes place with forming hollow carbon spheres. During the carbonization, sodium carbonate is melted and recrystallized as a hydrate particle. The recrystallization of sodium carbonate takes place at the inside of hollow carbon for the case of using PEG, whereas it proceeds at the whole surface for the case of using carbohydrazide with PEG. Finally, the ultrasonic washing removes the sodium carbonate hydrates. At this step, the hollow carbon (SP3), prepared from the spray solution containing PEG and carbohydrazide, are fractured to form carbon nanosheets because the very thin carbon layer is easy to be broken by a simple physical impact.

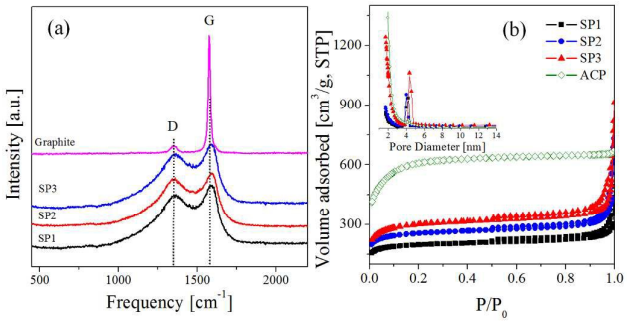

Fig. 6 (a) Raman spectra and (b) N_2 adsorption-desorption isotherms of the prepared carbon samples.

3.2 Raman and N_2 adsorption-desorption measurements

To investigate the structural information and the porosity of the obtained carbon powders, Raman spectroscopy and N_2 adsorption-desorption analysis were performed. Fig. 6a shows the Raman spectra for the carbon samples, SP1, SP2 and SP3. Graphitic carbons have two characteristic Raman peaks such as G and D bands. The G band is due to the first order scattering of the E_{2g} phonon of sp^2-hybridized C atoms, and the D band is ascribed to a breathing mode of κ-point photons of A_{1g} symmetry.[59] Usually, the G and D bands of graphite-structured carbon are found at around 1575 cm^{-1} and 1350 cm^{-1}, respectively. The Raman spectrum of a commercially available graphite sample was shown in Fig. 6a. The G and D bands of the graphite are observed at 1575 cm^{-1} and 1358 cm^{-1}, respectively. The prepared carbon samples have two intense peaks at 1358 cm^{-1} and 1607 cm^{-1}. The D bands of all prepared carbon samples are observed at the same position with the graphite. The G band of the

prepared carbons was observed at the longer wavenumber compared with the graphite. Given this, the prepared carbons have isolated double bonds. The relatively intense D band indicates that the carbons prepared have a small sp^2 domain size which is due to the existence of oxidation sites like graphene oxides. Therefore, from the Raman analysis, the prepared carbons are confirmed to have graphitic structure with isolated olefinic bonds (C=C) and small sp^2 domains like graphene. Fig. 6b shows the results of N_2 adsorption-desorption measurement. The isotherms of the prepared carbons are corresponding to a typical isotherm IV with a week hysteresis of type H3, indicating that the prepared carbon powders have mesoporous materials. The ACP sample shows a typical isotherm observed in microporous materials. The texture properties are summarized in Table 1. The specific surface areas are 2199, 669, 742 and 881 m^2/g for ACP, SP1, SP3 and SP3, respectively. The pore size distribution shown in the inset of Fig. 6b indicates that carbon particles prepared by spray pyrolysis have mesopores (4 – 5 nm). According to the N_2 isotherm, the carbon powders prepared using PEG or PEG/carbohydrazide mixture show an increase in the adsorption volume at below the relative pressure of $P/P_0 = 0.1$. As a result, the pore size distribution indicates that micropores less than 2 nm are increased when using the organic additives, especially for the SP3 carbon (nanosheet). That is, the decomposition of organic additives generates a lot of gaseous compounds which are contributed to form the micropores of carbon matrix. Given this, the use of organic additives is confirmed to be helpful for increasing the specific surface area of carbon particles prepared by the spray pyrolysis.

Table 1 Texture properties and specific capacitances for the porous carbon particles prepared by the ultrasonic spray pyrolysis process.

Sample name	Additives	S_{BET} [m^2/g]	V_p [cm^3/g]	D_{BJH} [nm]	Capacitance [F/g]	
					CV[b)]	EIS[c)]
ACP	-	2199	0.96	1.8	174	175
SP1	None	669	0.14	6.9	135	129
SP2	PEG	742	0.38	12.5	178	164
SP3	PEG+CH[a)]	879	0.74	5.7	206	195

a) Carbohydrazide; b) CV at 0.0 V; c) EIS at 20 mHz.

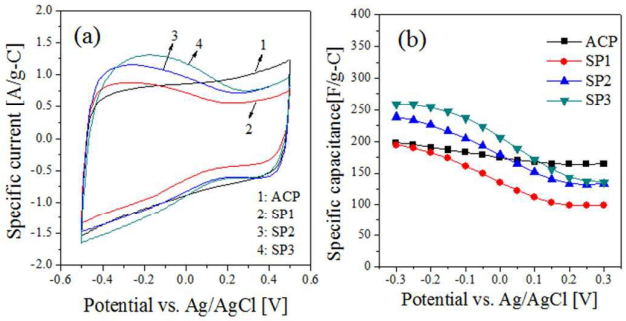

Fig. 7 (a) CV curves of electrodes prepared using the prepared carbon particles and (b) the specific capacitance as a function of applied voltage.

3.3 Electrochemical properties

The cyclic voltammetry (CV) and electrochemical impedance spectroscopy (EIS) were used to investigate the electrochemical performance of three carbon samples. Fig. 7a shows the CV curves for three electrodes fabricated using the prepared carbon SP1, SP2, SP3 and ACP. An ideal double-layer supercapacitor is known to have a rectangular-shaped CV curve. In a real situation, however, porous carbon electrodes have the combined hindrance of both Faradic current and ohmic resistance for the electrolyte diffusion. All the carbon electrodes have similar-shaped CV curves indicating that the adsorption and desorption of ions occurs efficiently. The SP3 carbon electrode shows the largest specific current, which means that the adsorption quantity of ions is largest. The specific capacitance (C) can be calculated from the CV data using the following equation.[43]

$$C = \frac{I_a - I_c}{2vm} \quad (1)$$

where I_a and I_b are the anodic and cathodic current (A) at the voltage (v), respectively. m is the mass of carbon. Fig. 7b is the specific capacitance as a function of the applied potential of -0.3 to +0.3V. For the prepared carbons, the SP3 carbon electrode has the largest capacitance at the all range of the applied potential. In special, the capacitance at the negative potential is larger than that at the positive potential. This result indicates that the prepared carbon particles have negative-charged functional groups. It is noteworthy that the SP2 and SP3 carbons show higher capacitance than the ACP electrode at the negative voltages. The specific capacitances calculated at 0.0V for the SP1, SP2 and SP3 carbons were summarized in Table 1. Compared with the SP1 (135 F/g), the specific capacitances of SP2 (178 F/g) and SP3 (206 F/g) are about 32 % and 53% enhanced, respectively. Especially, in spite of the smaller surface area, the SP3 electrode shows higher specific capacitance than that of the ACP electrode. This result indicates that the mesoporous carbon nanosheets prepared by the spray pyrolysis are more efficient compared with the microporous ACP for the application of ion sorption processes with a good cycling performance (Fig. S7).

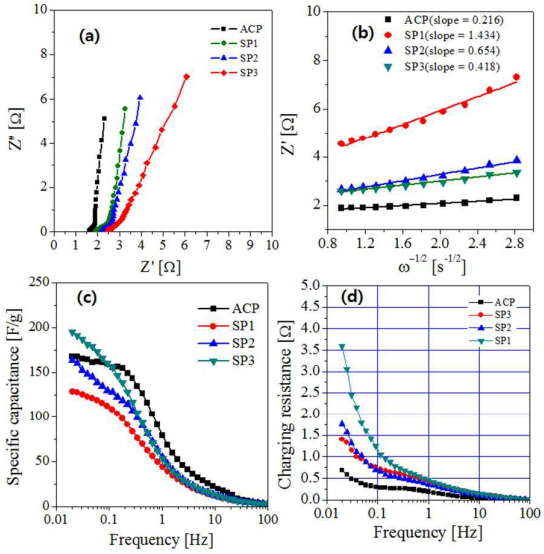

Fig. 8 EIS measurement results: (a) Nyquist plots, (b) the Z_{re} values as a function of $\omega^{-1/2}$, (c) specific capacitance, (d) charging resistance as a function of frequency.

Fig. 8a shows the Nyquist plots that show a nearly vertical curve. The prepared carbon electrodes show a capacitor response. In the low-frequency region, the slopes of vertical lines are changed with the type of carbon structures. The Z_{re} value (x-axis) in the low-frequency region has a linear relation with respect to $\omega^{-1/2}$. Herein, ω is the angular frequency expressed by $\omega = 2\pi f$. Fig. 8b shows the Z_{re} value as a function of $\omega^{-1/2}$. The slope of the straight line gives helpful information for the ion diffusion characteristics.[60-61] The small slope indicates that the diffusion rate of ions into porous electrodes is fast. Among the prepared carbons, the slope of carbon nanosheets (SP3) is smallest. Accordingly, the ion diffusion kinetics is better in the SP3 electrode than in the SP1 and SP2 electrodes. Therefore, the very thin carbon nanosheets (SP3) is proved to be more profitable structure than the porous carbon having hollow-structured (SP2) or filled-structured spherical shape (SP1) in terms of achieving high capacitance with good ionic sorption kinetics. Compared with the ACP electrode, however, the slope of the SP3 electrode is a little larger. This result reflects that ions are diffused more deeply into the inner surface of the carbon nanosheets whereas the ion adsorption mainly occurs on the surface region of microporous ACPs.

The double layer capacitance of carbon materials can be calculated from the imaginary value (Z'') of the Nyquist plots by the following equation.

$$C = \left| \frac{1}{2\pi f \times Z'' \times m} \right| \quad (2)$$

where f is the frequency. The resulting capacitances are shown in Fig. 8c. As the frequency decreases, the capacitance becomes increased because the ac-signal can charge more and more the inner surface sites of carbon electrodes. For the ACP electrode, the capacitance steeply increases with decreasing the frequency, and it is saturated at less than 0.2 Hz. That is, most of the surface sites involving in the ion sorption are charged at 0.2 Hz of the frequency. The SP1 electrode shows a similar response with that of the ACP electrode in the capacitance change with respect to the frequency. The SP2 or SP3 electrode, however, the capacitance increases steadily with decreasing the frequency. This result indicates that the ac-signal is propagated deeply to the inside pore surfaces of the SP2 or SP3 carbons. As the ac-signal is propagated into inner surfaces of porous carbons, the electrolyte diffusion path is elongated. As a result, the real component (Z') of the impedance will be increased. The charging resistance can be calculated from the increment in the real part of the impedance from the resistance at 100 Hz. Fig. 8d shows the resulting charging resistance. At the frequency below 0.1 Hz, the charging resistance shows large difference. The charging resistance of the SP2 and SP3 electrodes is much smaller compared with the SP1 electrode, but it is still larger than the ACP electrode. The charging resistance can be connected with the diffusion path of ions. That is, the large charging resistance reflects that the diffusion path of ions is long and complicated. Consequently, the carbon nanosheets (SP3) or hollow spherical carbons (SP2) have shorter and simpler pore structure compared with the porous spherical-shaped carbons (SP1). The characteristics of the charging resistances are in good agreement with the results of ion diffusion kinetics as shown in Fig. 8b.

The specific capacitance of carbon materials will increase proportionally to the increase of the surface area if the entire surface is involved in the ionic sorption. In a real situation, however, the ionic elements cannot access to the entire surface. As a result, the effective surface area involved in ionic sorption is more important than the total surface area. In order to serve the surface for electrosorption, an electrical double layer should be formed within the pores of carbon electrodes. To do this, the pore size should be larger than a cutoff pore width (w_m) at which the surface charge density is zero.[62] If the pores are smaller than w_m, the electrical double layer is overlapped so that the pore surface cannot be involved in the electrosorption of ions. That is, the inside micropores of carbon electrodes could not contribute to the ionic sorption. Consequently, the external surface or the mesopores play substantially important role in the electrosorption process. As shown in Table 1, the specific surface areas of SP2 and SP3 carbons are about 11% and 31% larger than the SP1 carbon. The increment in the specific capacitance is larger than that in the surface area. This result says that the surface fraction taking part in the ionic sorption is larger in the SP2 (hollow) and SP3 (nanosheet) carbons than in the SP1 carbon. The SP3 carbon has the specific surface area about 18% larger than the SP2 carbon, and the specific capacitance is 16% larger. Given this, the very hollow carbon with a thin layer compared with mesoporous spherical carbon having a filled structure is advantage to increase the substantial surface area to take part in the ionic sorption. Furthermore, the carbon nanosheet having a similar structure with a multi-layered graphene is better than the hollow-structure carbon in terms of improving the ionic-sorption capacitance. ACPs have much larger specific surface area than carbon nanosheets prepared by spray pyrolysis. Nevertheless, the specific capacitance of carbon nanosheets is larger than that of ACPs. This result indicates that the active surface area substantially involving in the ion adsorption is larger in mesoporous carbon nanosheets compared with micro-porous ACPs.

4. Conclusions

In the present work, the porous carbons with different morphology were synthesized by spray pyrolysis. A new and easy strategy to prepare hollow and nanosheet carbon powders via spray pyrolysis was suggested, and its superior performance for ionic sorption was proved experimentally. The morphology and nanostructure were easily controlled only by adding organic additives (PEG or carbohydrazide) to the sucrose-based aqueous solution. The hollow-structured carbon spheres were obtained by adding PEG to the spray solution. When carbohydrazide with PEG was used as the organic additive, the resulting carbon powders had a nanosheet shape with a very thin thickness like multi-layered graphene oxides. According to the Raman analysis, all the carbon particles prepared by the spray pyrolysis had a graphitic structure with isolated olefinic bonds (C=C), which was not affected by the use of organic additives. The addition of organic additives was also helpful for increasing the specific surface area. As a result, the surface area of carbon nanosheets prepared by adding both PEG and carbohydrazide increased about 31% compared with the spherical porous carbon prepared without any organic additives. From the electrochemical analysis, the hollow-structured carbon or the carbon nanosheet powders had higher ion-sorption capacitance compared with the spherical-shaped mesoporous carbon powders due to the increase of ion-accessible surface area. The thin-nanosheet carbon powders, which can be easily synthesized by the suggested spray pyrolysis, were revealed to have the highest ion-sorption capacitance and expected to be potentially applicable as electrode materials for supercapacitor, battery and capacitive deionization.

Acknowledgements

This research was supported by Basic Science Research Program through the National Research Foundation of Korea (NRF) funded by the Ministry of Science, ICT & Future Planning (Grant No. 2015R1A2A2A03006558).

Notes and references

‡ Footnotes relating to the main text should appear here. These might include comments relevant to but not central to the matter under discussion, limited experimental and spectral data, and crystallographic data.
§
§§
etc.

1 J. M. Tarascon and M. Armand, *Nature*, 2001, **414**, 359.
2 M. Endo, C. Kim, K. Nishimura, T. Fujino and K. Kiyashita, *Carbon*, 2000, **38**, 183.
3 Y. P. Wu, E. Rahm and R. Holze, *J. Power Sources*, 2003, **114**, 228.
4 F. Zheng, G. Xia, Y. Yang and Q. Chen, *Nanoscale*, 2015, **7**, 9637.
5 F. Zietzchmann, J. Altmann, C. Hannemann and M. Jekel, *Water Res*., 2015, **83**, 52.
6 J. Wang and Q. Liu, *Nanoscale*, 2014, **6**, 4148.
7 N. Djafarzadeh, M. Safarpour and A. Khataee, *Korean J. Chem. Eng*., 2014, **31**, 785.
8 J. Gong, J. Liu, X. Chen, Z. Jiang, X. Wen, E. Mijowska and T. Tang, *J. Mater. Chem. A*, 2015, **3**, 341.
9 F. Rodriguez-Reinoso, *Carbon*, 1998, **36**, 159.
10 J. Klein, D. Wu, V. Tschamber, I. Fechete, F. Garin, *Appl. Catal. B-Environ*., 2013, **132-133**, 527.
11 J. Cheng, Y. Wang, C. Teng, Y. Shang, L. Ren and B. Jiang, *Chem. Eng. J*., 2014, **242**, 285.
12 B. P. Vinayan, N. I. Schwarzburger and M. Fichtner, *J. Mater. Chem. A*, 2015, **3**, 6810.
13 Y. Bai, Z. Wang, C. Wu, R. Xu, F. Wu, Y. Liu, H. Li, Y. Li, J. Lu and K. Amine, *ACS Appl. Mater. Inter*., 2015, **7**, 5598.
14 Y. Gong, M. Zhang and G. Cao, *RSC Adv*., 2015, **5**, 26521.
15 X. Y. Chen, H. Song, Z. J. Zhang and Y. Y. He, *Electrochim. Acta*, 2014, 117, 55.
16 C. Guan, J. Liu, Y. Wang, L. Mao, Z. Fan, Z. Shen, H. Zhang and J. Wang, *ACS Nano*, 2015, **9**, 5198.
17 T. X. Shang, X. X. Cai and X. J. Jin, *RSC Adv*., 2015, **5**, 16433.
18 A. Thambidurai, J. K. Lourdusamy, J. V. John and S. Ganesan, *Korean J. Chem. Eng.*, 2014, **31**, 268.
19 C. Tsouris, R. Mayes, J. Kiggans, K. Sharma, S. Yiacoumi, D. DePaoli and S. Dai, *Environ. Sci. Technol*., 2011, **45**, 10243.
20 S. Porada, P. M. Biesheuvel and V. Presser, *Adv. Funct. Mater*., 2015, **25**, 179.
21 H. Wang, L. Shi, T. Yan, J. Zhang, Q. Zhong and D. Zhang, *J. Mater. Chem. A*, 2014, **2**, 4739.
22 Y. Liu, C. Nie, X. Liu, X. Xu, Z. Sun and L. Pan, *RSC Adv*., 2015, **5**, 15205.
23 L. Wang, G. Mu, C. Tian, L. Sun, W. Zhou, P. Yu, J. Yin and H. Fu, *ChemSusChem*, 2013, **6**, 880.
24 L. Whang, G. Mu, C. Tian, L. Sun, W. Zhou, T. Tan and H. Fu, *ChemSusChem*, 2012, **5**, 2442.
25 L. Wang, L. Sun, C. Tian, G. Mu, H. Zhang and H. Fu, *RSC Adv*., 2012, **2**, 8359.
26 F. Rodriguez-Reinoso, *Handb. Porous Solids*, 2002, **3**, 1766.
27 Z. Hu and E. F. Vansant, *Carbon*, 1995, **33**, 561.
28 M. S. Tam and M. J. Antal, *Ind. Eng. Chem. Res*., 1999, **38**, 4268.
29 H. Tamon, H. Ishizaka, M. Mikami and M. Okazaki, *Carbon*, 1997, **35**, 791.
30 R. Ryoo, S. H. Joo and S. Jun, *J. Phys. Chem. B*, 1999, **103**, 7743.
31 J. Lee, S. Han and T. Hyeon, *J. Mater. Chem*., 2004, **14**, 478.
32 Z.-A. Qiao, B. Guo, A. J. Binder, J. Chen, G. M. Veith, and S. Dai, *Nano Lett.*, 2013, **13**, 207.
33 Y. Jiang, Y. Wang, Y. Zhang, X. Shu, Z. Chen and Y.-C. Wu, *J. Solid State Electrochem*., 2015, **19**, 3087.
34 Y. Seo, K. Kim, Y. Jung and R. Ryoo, Micropor. Mesopor. Mater., 2015, 207, 156.
35 J. Kong, A. M. Cassell and H. Dai, *Chem. Phys. Lett*., 1998, **292**, 567.
36 Z. Li, P. Wu, C. Wang, X. Fan, W. Zhang, X. Zhai, C. Zeng, Z. Li, J. Yang and J. Hou, *ACS Nano*, 2011, **5**, 3385.
37 Y. Zhao, J. Choi, P. Kim, W. Fei and C. J. Lee, *RSC Adv*., 2015, **5**, 30564.
38 Q. Hu, Y. Fu and G. P. Meisner, *J. Phys. Chem. C*, 2008, **112**, 1516.
39 S. E. Skrabalak, *Phys. Chem. Chem. Phys*., 2009, **11**, 4930.
40 M. E. Fortunato, M. Rostam-Abadi and K. S. Suslick, *Chem. Mater*., 2010, **22**, 1610.
41 J. Guo and K. S. Suslick, *Chem. Commun*., 2012, **48**, 11094.
42 K. Sohn, Y. J. Na, H. Chang, K.-M. Roh, H. D. Jang and J. Huang, *Chem. Commun*., 2012, **48**, 5968.
43 V. Etacheri, C. Wang, M. J. O'Connell, C. K. Chan and V. G. Pol, *J. Mater. Chem. A*, 2015, **3**, 9861.
44 C. Wang, Y. Wang, J. Graser, R. Zhao, F. Gao and M. J. O'Connell, *ACS Nano*, 2013, **7**, 11156.
45 Y. N. Ko, S. B. Park, K. Y. Jung and Y. C. Kang, *Nano Lett*., 2013, **13**, 5462.
46 N. Jo, J.-H. Choi and K. Y. Jung, *J. Electrochem. Soc*., 2013, **160**, E84.
47 A. F. Arif, R. Balgis, T. Ogi, T. Mori and K. Okuyama, *Chem. Eng. J*., 2015, **271**, 79.
48 J. S. Cho, K. Y. Jung and Y. C. Kang, *Phys. Chem. Chem. Phys*., 2015, **17**, 1325.
49 J. S. Cho, S. M. Lee, K. Y. Jung and Y. C. Kang, *RSC Adv*., 2014, **4**, 43606.
50 J. H. Kim and K. Y. Jung, *J. Lumin*., 2011, **131**, 1487.
51 J. W. Overcash and K. S. Suslick, *Chem. Mater*., 2015, **27**, 3564.
52 H. R. Jang, H.-J. Oh, J.-H. Kim and K. Y. Jung, *Micropor. Mesopor. Mater*., 2013, **165**, 219.

53 K. Y. Jung, Y. R. Jung, J.-K. Jeon, J. H. Kim, Y.-K. Park and S. Kim, *J. Ind. Eng. Chem*., 2011, **17**, 144.

54 G. D. Park, J. S. Cho and Y. C. Kang, *ACS Appl. Mater. Inter.*, 2015, **7**, 16842.

55 D. Kotsikau, M. Ivanovskaya, V. Pankov and Y. Fedotova, *Solid State Sci*., 2015, **39**, 69.

56 S. H. Choi, D. S. Jung, J. W. Choi and Y. C. Kang, *Chem.-Eur. J*., 2015, **21**, 2076.

57 D. S. Jung, T. H. Hwang, J. H. Lee, H. Y. Koo, R. A. Shakoor, R. Kahraman, Y. N. Jo, M.-S. Park and J. W. Choi, *Nano Lett*., 2014, **14**, 4418.

58 H. Xu, J. Guo and K. S. Suslick, *Adv. Mater*., 2012, **24**, 6028.

59 A. C. Ferrari, J. C. Meyer, V. Scardaci, C. Casiraghi, M. Lazzeri, F. Mauri, S. Piscanec, D. Jiang, K. S. Novoselov, S. Roth and A. K. Geim, *Phys. Rev. Lett*., 2006, **97**, 187401.

60 S. H. Choi, K. Y. Jung and Y. C. Kang, *ACS Appl. Mater. Inter*., 2015, **7**, 13952.

61 S. Yang, X. Wang, X. Yang, Y. Bai, Z. Liu, H. Shu and Q. Wei, *Electrochim. Acta*, 2012, **66**, 88.

62 K.-L. Yang, T.-Y. Ying, S. Yiacoumi, C. Tsouris and E. S. Vittoratos, *Langmuir*, 2001, **17**, 1961.

The table of contents entry

We developed a new synthetic strategy which can easily control the particle morphology and microstructure of carbon particles via an ultrasonic spray pyrolysis. For the first time, porous carbon nanosheets with high ion-sorption capacitance were prepared by the one-pot spray pyrolysis process.